

Shadows of a generic class of spherically symmetric, static spacetimes

Md. Golam Mafuz,^{1,*} Rishank Diwan,^{2,3,†} Soumya Jana,^{4,2,‡} and Sayan Kar^{2,§}

¹*Department of Physics, Jadavpur University, Kolkata, 700032, India*

²*Department of Physics, Indian Institute of Technology Kharagpur, 721 302, India*

³*Laboratory for Space Research, The University of Hong Kong, Hong Kong*

⁴*Department of Physics, Sitananda College, Nandigram, 721631, India*

Abstract

We explore the characteristics of shadows for a general class of spherically symmetric, static spacetimes, which may arise in general relativity or in modified theories of gravity. The chosen line element involves a sum (with constant but different coefficients) of integer powers of $\frac{1}{r}$ in g_{tt} and g_{rr} , in the Schwarzschild gauge. We begin our discussion by motivating the line element through a study of the energy conditions (null and weak) and the extent to which they are satisfied/violated for diverse choices of the parameters appearing in the metric functions. Subsequently, we construct the circular shadows and analyse the dependence of the shadow radius on the metric parameters. We find that with specific choices of the metric parameters (within the ranges allowed by the energy conditions) one can, in principle, obtain values that conform with recent observations on shadows, as available in the literature. We also mention where such metrics may arise (i.e., in which theory of gravity and the physical scenario therein), thereby proposing that the observed shadows may be representative signatures of different theoretical contexts.

* Email Address: golammafuzgm@gmail.com

† Email Address: rishank2610@gmail.com

‡ Email Address: soumyajana.physics@gmail.com (Corresponding author)

§ Email Address: sayan@phy.iitkgp.ac.in (Corresponding author)

I. INTRODUCTION

The recent observations of shadows of M87* [1–5] and SgrA* [6–11] by the EHT collaboration have opened up the new possibility of probing a highly dynamical region of strong gravity in the vicinity of a supermassive black hole/ compact object . A black hole’s shadow [12] (also known as a silhouette [13, 14]) is the apparent (i.e., gravitationally lensed) image of the photon sphere (a region of spacetime where photons move along unstable orbits), appearing as a two-dimensional dark zone in the observer’s sky [14–16]. Strong gravitational lensing of light rays near the photon sphere is important for distinguishing between the spacetime structures of black holes and other compact objects [17–22]. Synge’s (1966) seminal study defined the angular radius of the photon capture areas bordering the Schwarzschild black hole [23]. Later, Bardeen explored the Kerr black hole’s shadow and observed that the spin would deform the shape of the shadow [24]. Luminet (1979) [25] established through simulations that the photon capture radius of a black hole surrounded by a geometrically thin, optically thick accretion disc would appear to a distant observer as a thin emission ring inside a lensed image. Since then, much effort has gone into expanding our knowledge of how to quantify black hole shadows in known spacetimes employing general relativity (GR) [26–33]. Furthermore, the notion of shadows has also been analysed for black holes in extended gravity theories [34–40], for other compact objects [41–43], for black hole surrounded by dark matter [44], etc. Observational results on black hole shadows are being used to validate theoretical/computational findings on the shadow radius, shadow profile as well as astrophysical processes in the strong-field regime (see [45–48]). For reviews one may look at [49] and [16]. As mentioned before, one may constrain the parameters in the black hole solutions in different alternative theories of gravity using concrete facts and numbers emerging from shadow images [50, 51]. Apart from the Schwarzschild solution, the Reissner-Nordstrom (RN) [52, 53] metric is the next most basic example within the class of metrics to be discussed in this article. Articles in [54, 55] investigated the effect of including a quadratic in the $\frac{1}{r}$ term as found in the standard RN solution. Moreover, in many alternative theories of gravity, there exist static, spherically symmetric solutions involving a sum (with constant but distinct coefficients) of integer powers of $\frac{1}{r}$ in g_{tt} and g_{rr} , in the Schwarzschild gauge. Some examples appear in [56, 57] (see also [58] for consequences of extensions of this theory) [59, 60], [61–63], [64](see [65] for a recent revisit on this metric),

and [66, 67]. The above-mentioned examples of such line elements motivates us to investigate, in a broad sense, a general static spherically symmetric metric in the Schwarzschild gauge, involving a sum (with constant but different coefficients) of integer powers of $\frac{1}{r^n}$ upto $n = 4$, in $g_{tt} = -g_{rr}^{-1}$. We address (i) the violation/satisfaction of the energy conditions for the ‘matter’ (assuming *GR*-like equations) required to support these spacetimes and (ii) the shadow profiles for the above static, spherically symmetric geometries. In both (i) and (ii) our main goal is to find how the choice of the range of values of the metric parameters influence the consequences. We also use current observational/imaging results to set bounds on the parameters, which, in turn, can constrain the theory (when other than GR). In the end, we provide a couple of specific results for metric functions which may contain a sum of N terms (arbitrary but finite N). While discussing the energy conditions, we have chosen to use the Weak and Null Energy Conditions, abbreviated as WEC and NEC. It is assumed at the outset that our generic line elements are ‘solutions’ in General Relativity or any modified theory in which the Einstein or Einstein-like equations $G_{\alpha\beta} = \kappa T_{\alpha\beta}^{\text{eff}}$ hold. As a result, the ‘required matter’ that can be found from $G_{\alpha\beta}$ must necessarily be examined for the satisfaction/violation of the energy condition inequalities. In a way, we are actually looking at the ‘convergence conditions’ (timelike/null). What we broadly call ‘matter’ in our analysis, may include ‘other’ quantities eg. an ambient scalar (like in Brans-Dicke theory). Our article is divided into six sections. Section II introduces the metrics and comments on the parameters that appear in them. Section III is devoted to the energy conditions (both Weak and Null) for the metrics under consideration. Section IV delves into the nature of black hole shadows. Following this, in Section V, we investigate the nature of values for the metric parameters, in the context of current shadow observations. In section VI we discuss some results on a more general metric (arbitrary but finite n). Finally, in Section VII, we summarise our findings and discuss potential consequences. Throughout the paper we assume $G = c = 1$ and the metric signature convention $(-, +, +, +)$.

II. THE CLASS OF STATIC, SPHERICALLY SYMMETRIC SPACETIMES

As mentioned before, we will be concerned with a generic line element of the following form:

$$ds^2 = g_{\alpha\beta} dx^\alpha dx^\beta = - \left[1 + \frac{\mathcal{P}}{r} + \frac{\mathcal{Q}}{r^2} + \frac{\mathcal{S}}{r^3} + \frac{\mathcal{T}}{r^4} \right] dt^2 + \left[1 + \frac{\mathcal{P}}{r} + \frac{\mathcal{Q}}{r^2} + \frac{\mathcal{S}}{r^3} + \frac{\mathcal{T}}{r^4} \right]^{-1} dr^2 + r^2 d\Omega_2^2 \quad (2.1)$$

where $\mathcal{P}, \mathcal{Q}, \mathcal{S}, \mathcal{T}$ are constants. We could have kept powers upto say $\frac{1}{r^N}$, for a general N . However, it is difficult to say anything concrete for arbitrary N – hence our restriction to $N = 4$. Numerous examples of metrics of the above form appear in GR or modified theories of gravity. We mention some of these below in order to motivate our approach and calculations. We will return to some comments on general N in the penultimate section of the article.

Our first example is the ‘4-component’ generalized Kiselev spacetime [64] given by the following line element

$$ds^2 = - \left[1 - \frac{\sum_{i=1}^4 K_i r^{-3w_i}}{r} \right] dt^2 + \left[1 - \frac{\sum_{i=1}^4 K_i r^{-3w_i}}{r} \right]^{-1} dr^2 + r^2 d\Omega_2^2 \quad (2.2)$$

where $d\Omega_2^2 = d\theta^2 + \sin^2 \theta d\phi^2$ is the line element corresponding to a 2-sphere. In the above metric, K_i ’s are constants containing the parameters appearing in the metrics considered here. We absorb any Schwarzschild mass term present into one of the K_i by setting the corresponding w_i to zero. Thus, essentially, following [65, 68], we define a position-dependent mass function $m(r)$ of the form

$$2m(r) = \sum_{i=1}^4 K_i r^{-3w_i} \quad (2.3)$$

Comparing the two line elements in equation (2.1) and (2.2), we have w_i ’s as follows: $w_1 = 0, w_2 = \frac{1}{3}, w_3 = \frac{2}{3}, w_4 = 1$, and K_i ’s as: $\mathcal{P} = -K_1, \mathcal{Q} = -K_2, \mathcal{S} = -K_3, \mathcal{T} = -K_4$. Originally, the Kiselev spacetime was obtained as a solution in GR for quintessence matter surrounding a black hole. However, the Kiselev-type solutions also exist in other contexts such as GR coupled with nonlinear electrodynamics [69] and black holes surrounded by fluids in $f(R, T)$ gravity [70].

The second example stems from early work in braneworld gravity. An interesting braneworld solution is the tidal Reissner-Nordström (tidal-RN) braneworld black hole solution [67, 71]

$$ds^2 = - \left[1 - \frac{2M}{r} + \frac{Q}{r^2} \right] dt^2 + \left[1 - \frac{2M}{r} + \frac{Q}{r^2} \right]^{-1} dr^2 + r^2 d\Omega_2^2 \quad (2.4)$$

The above solution has the form of the Reissner-Nordström (RN) solution of GR with no electric field present on the brane. Q is a tidal charge parameter arising from the Weyl tensor of the bulk. Unlike in the RN case, Q can be both positive and negative [67].

The static black hole solutions of the field equations for the quartic Horndeski square root Lagrangian [57] constitute our third example. The line element is given as:

$$ds^2 = - \left[1 - \frac{\mu}{r} - \frac{\beta^2}{2\zeta\eta r^2} \right] dt^2 + \left[1 - \frac{\mu}{r} - \frac{\beta^2}{2\zeta\eta r^2} \right]^{-1} dr^2 + r^2 d\Omega_2^2 \quad (2.5)$$

where μ is a free integration constant, η and β are dimensionless parameters, and $\zeta = \frac{M_{\text{Pl}}}{16\pi}$. The above solution describes a black hole with mass $\frac{\mu}{2}$.

Our fourth example is that of a magnetically charged black hole solution obtained in Extended-Scalar-Tensor-Gauss-Bonnet gravity coupled with nonlinear electrodynamics [72]. The black hole spacetime is given by

$$ds^2 = - \left[1 - \frac{2M}{r} - \frac{q^3}{r^3} \right] dt^2 + \left[1 - \frac{2M}{r} - \frac{q^3}{r^3} \right]^{-1} dr^2 + r^2 d\Omega_2^2, \quad (2.6)$$

where M is the mass of the black hole and q is the scalar charge and related to the magnetic charge of the black hole $Q_m = \sqrt{2}q$. The spacetime is completely different from the Reissner-Nordström- type black holes but falls under the general class that we consider here. The presence of the $\frac{1}{r^3}$ term in the metric functions is a point to note here.

Finally, consider the metric for the black hole surrounded by dust in Rastall theory of gravity given by [73],

$$ds^2 = - \left[1 - \frac{2M}{r} + \frac{Q}{r^2} + \frac{N_d}{r^{\frac{1-6\kappa\lambda}{1-3\kappa\lambda}}} \right] dt^2 + \left[1 - \frac{2M}{r} + \frac{Q}{r^2} + \frac{N_d}{r^{\frac{1-6\kappa\lambda}{1-3\kappa\lambda}}} \right]^{-1} dr^2 + r^2 d\Omega_2^2 \quad (2.7)$$

One can realize that in GR, i.e. in the limit of $\lambda \rightarrow 0$ and $\kappa = 8\pi G$, the black hole in the dust background appears as a charged black hole with an effective mass $M^{\text{eff}} = M - N_d/2$. Thus, we see that for $\kappa\lambda \neq 0$, the geometric parameters κ and λ of the Rastall theory can play an important role leading to distinct solutions relative to GR. One can realize that for $\kappa\lambda \neq 0$, the Rastall correction term never behaves as the mass or charge terms, and introduces a new character to the black hole.

We have provided some examples of scenarios in GR or modified gravity where a metric of the form similar to equation (2.1) arises. There are many more which one can find in the literature. Each of these line elements can be viewed as ‘solutions’ of equations like $G_{\alpha\beta} = \kappa T_{\alpha\beta}^{\text{eff}}$, where the R.H.S. is an effective matter stress energy which contains usual matter plus an ‘effective’ stress energy whose origins could be geometric or anything else. We now move on to discuss the energy conditions of this $T_{\alpha\beta}^{\text{eff}}$ which can be written down from the Einstein tensor for the general line element in equation (2.1).

III. ENERGY CONDITIONS

The Weak Energy Condition (WEC) [74, 75] states that the matter energy density measured by any observer in a spacetime is never negative and we may represent it in the following form

$$T_{\alpha\beta} v^\alpha v^\beta \geq 0 \quad (3.1)$$

where v^α, v^β are any future-directed timelike vectors. For a diagonal stress-energy tensor $T_{\alpha\beta}$, the WEC in a static observer's frame implies

$$\rho \geq 0 \quad \text{and} \quad \rho + \tau_i \geq 0, \quad i = 1, 2, 3 \quad (3.2)$$

The Null Energy Condition (NEC) refers to the following inequality

$$T_{\alpha\beta} k^\alpha k^\beta \geq 0 \quad (3.3)$$

where k^α, k^β are arbitrary, future-directed null vectors. The NEC for a diagonal stress-energy tensor in a static observer's frame corresponds to

$$\rho + \tau_i \geq 0, \quad i = 1, 2, 3 \quad (3.4)$$

In Eqs. (3.2) and (3.4), ρ is the density of mass-energy, τ_1 is radial pressure, τ_2 and τ_3 are tangential pressures. Since the Einstein field equations demand that the stress-energy tensor be proportional to Einstein tensor, in the static observer's frame the stress-energy tensor $T_{\hat{\alpha}\hat{\beta}}$ should have the same algebraic structure as the Einstein tensor $G_{\hat{\alpha}\hat{\beta}}$. Thus, $T_{\hat{t}\hat{t}} = \rho$, $T_{\hat{r}\hat{r}} = \tau_1$ and $T_{\hat{\theta}\hat{\theta}} = T_{\hat{\phi}\hat{\phi}} = \tau_2 = \tau_3$, are the only non zero components of the stress-energy tensor [74-76] into a perfect fluid [77]. The energy conditions (assuming $T_{\alpha\beta} = \frac{1}{\kappa} G_{\alpha\beta}$) in the proper reference frame for this metric are the following in-equalities (ignoring the overall positive factor $\frac{1}{\kappa}$):

$$\rho = \frac{r^2 \mathcal{Q} + 2r \mathcal{S} + 3\mathcal{T}}{r^6} \geq 0 \quad (3.5)$$

$$\rho + \tau_2 = \frac{2r^2 \mathcal{Q} + 5r \mathcal{S} + 9\mathcal{T}}{r^6} \geq 0 \quad (3.6)$$

A crucial point to note here is that $\rho + \tau_1 = 0$ for all r and all values of the parameters. We also infer the following points from the inequalities:

- (a) The inequalities are independent of the parameter \mathcal{P} .
- (b) For $\mathcal{Q} > 0$, $\mathcal{S} > 0$, $\mathcal{T} > 0$ both inequalities hold for all r . Thus WEC and NEC hold for

all r .

(c) For $\mathcal{Q} > 0$, $\mathcal{S} < 0$, $\mathcal{T} > 0$ both inequalities hold, for all r , if $\mathcal{S}^2 < \frac{72}{25}\mathcal{Q}\mathcal{T}$. This requirement (i.e. $\mathcal{S}^2 < \frac{72}{25}\mathcal{Q}\mathcal{T}$) follows from the condition for which the roots of the equalities are complex conjugate pairs. One can check that the minimum value of the numerator factor in the R. H. S. of both the inequalities (subject to appropriate choices of \mathcal{Q} , \mathcal{R} and \mathcal{T}) is positive definite.

(d) Other combinations of \mathcal{Q} , \mathcal{S} and \mathcal{T} may lead to the WEC, NEC being satisfied over restricted ranges. For example one can write both the numerators as products of the form $(r - r_+)(r - r_-)$. Among the four values of the roots, if one chooses the largest, then if r is greater than this largest root, both WEC, NEC will hold in that domain of r .

(e) For $\mathcal{Q} < 0$ the energy conditions are violated for large r irrespective of any values of \mathcal{S} , \mathcal{T} . For $\mathcal{Q} < 0$, $\mathcal{S} > 0$, $\mathcal{T} < 0$ violation of the energy conditions occur for all r when $\mathcal{S}^2 < \frac{72}{25}\mathcal{Q}\mathcal{T}$, whereas if $\mathcal{S}^2 > \frac{72}{25}\mathcal{Q}\mathcal{T}$ there exists only the intermediate region of space $r_- < r < r_+$ where the energy conditions are satisfied. Also, for $\mathcal{Q} < 0$, $\mathcal{S} < 0$, $\mathcal{T} < 0$ the energy conditions are violated at any r .

In Table I, we summarise the status of NEC and WEC for all possible positive or negative combinations of \mathcal{Q} , \mathcal{S} , \mathcal{T} . Fig. 1 demonstrates the status of the energy conditions with reference to the available parameter space. This status is shown via coloured regions in the plots for s vs. t (where $s = \mathcal{S}/M^3$ and $t = \mathcal{T}/M^4$) for $\mathcal{Q} > 0$ and $\mathcal{Q} < 0$. In the green region, NEC and WEC are satisfied for all r . In the yellow region the energy conditions are partially satisfied for restricted r , whereas the grey region indicates the violation of the energy conditions at all r . Thus, the figure provides an overall summary of the details shown in Table I.

Let us now move on to illustrate the L. H. S. of the energy condition inequalities for different sets of values for the parameters $\{\mathcal{P}, \mathcal{Q}, \mathcal{S}, \mathcal{T}\}$. We need not fix \mathcal{P} since it does not appear in the inequalities. We will rename $\mathcal{P} = -2M$. The remaining \mathcal{Q} , \mathcal{S} , \mathcal{T} are chosen to satisfy the constraints mentioned above. In order to deal with dimensionless quantities we write

$$\bar{r} = \frac{r}{M} \quad ; \quad \mathcal{Q} = qM^2 \quad ; \quad \mathcal{S} = sM^3 \quad ; \quad \mathcal{T} = tM^4 \quad (3.7)$$

where q, s, t are numbers. The two inequalities rewritten in terms of the new variables become

$$\rho = \frac{q\bar{r}^2 + 2s\bar{r} + 3t}{M^2\bar{r}^6} \geq 0 \quad ; \quad \rho + \tau_2 = \frac{2q\bar{r}^2 + 5s\bar{r} + 9t}{M^2\bar{r}^6} \geq 0 \quad (3.8)$$

We plot (Figure 2) only the numerators of the above inequalities in order to verify their

| \mathcal{Q} | \mathcal{S} | \mathcal{T} | NEC and WEC status |
|---------------|---------------|---------------|---|
| + | + | + | satisfied for all r |
| + | + | - | satisfied for $r > r_{+,max}$ |
| + | - | + | satisfied for all r when $\mathcal{S}^2 \leq \frac{72}{25}\mathcal{Q}\mathcal{T}$; violation occur at $r_{-,min} < r < r_{+,max}$ when $\mathcal{S}^2 > \frac{72}{25}\mathcal{Q}\mathcal{T}$ |
| + | - | - | violation in between $r_{-,min} < r < r_{+,max}$, satisfied elsewhere |
| - | + | + | satisfied only for $r_{-,2nd} < r < r_{+,2nd}$ |
| - | + | - | violation for all r when $\mathcal{S}^2 \leq \frac{72}{25}\mathcal{Q}\mathcal{T}$; satisfied only at $r_{-,2nd} < r < r_{+,2nd}$ when $\mathcal{S}^2 > \frac{72}{25}\mathcal{Q}\mathcal{T}$ |
| - | - | + | violation occur at $r \geq r_{+,2nd}$ |
| - | - | - | violation for all r |

TABLE I: NEC and WEC validity/violation are tabulated for different signatures of \mathcal{Q} , \mathcal{S} , \mathcal{T} . Here $r_{+,max}$ and $r_{-,min}$ denote the largest and the smallest among all roots of the numerators of the L.H.S. of Eqs. (3.5) and (3.6) and $r_{+,2nd}$ and $r_{-,2nd}$ are the second largest and second smallest among all the roots.

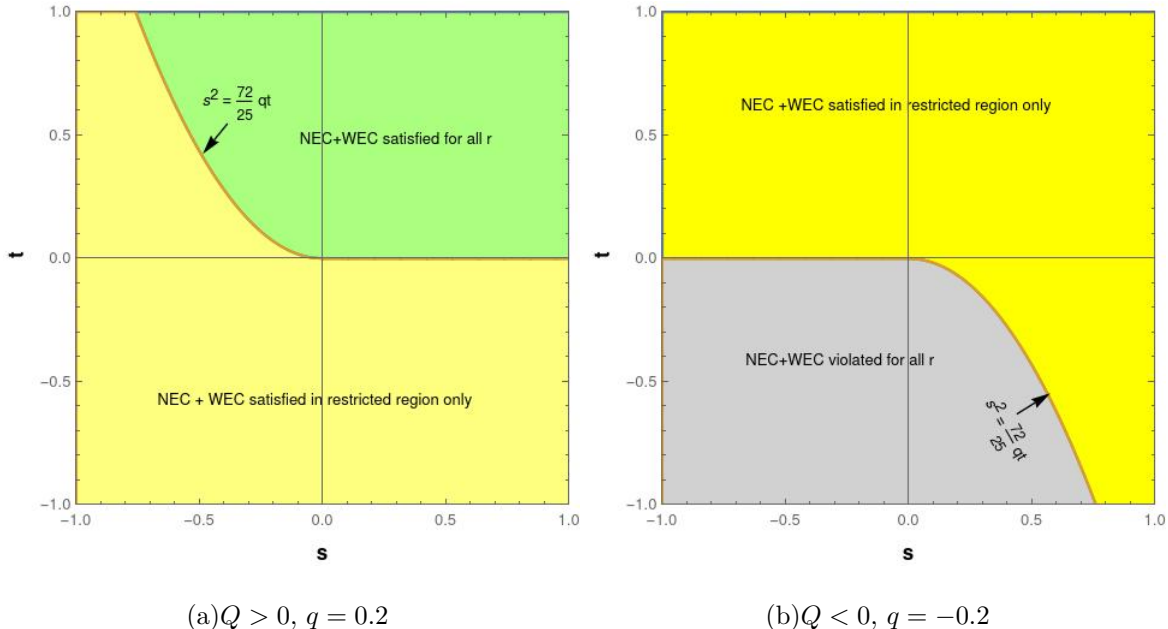


FIG. 1: $t - s$ region plot (for a fixed q) showing the status of NEC and WEC. In the left panel (a) $q = \mathcal{Q}/M^2 > 0$. We choose a particular value $q = 0.2$ to specify the boundary $s^2 = \frac{72}{25}qt$. However, the nature of the plot does not change for any other positive value of q . In the right panel (b) $q = \mathcal{Q}/M^2 < 0$. We choose a particular value $q = -0.2$

positivity for all r . The triplet (q, s, t) are chosen as $(2, -1, 3)$ (energy condition satisfying) and $(1, -2, 1)$ (energy condition violating) – these values are considered with the sole aim of illustration. In general, as mentioned earlier, if required conditions are met, one is sure of satisfying the energy conditions. Later we will try to correlate the shadow radius with scenarios of metrics for which the required matter satisfies WEC, NEC.

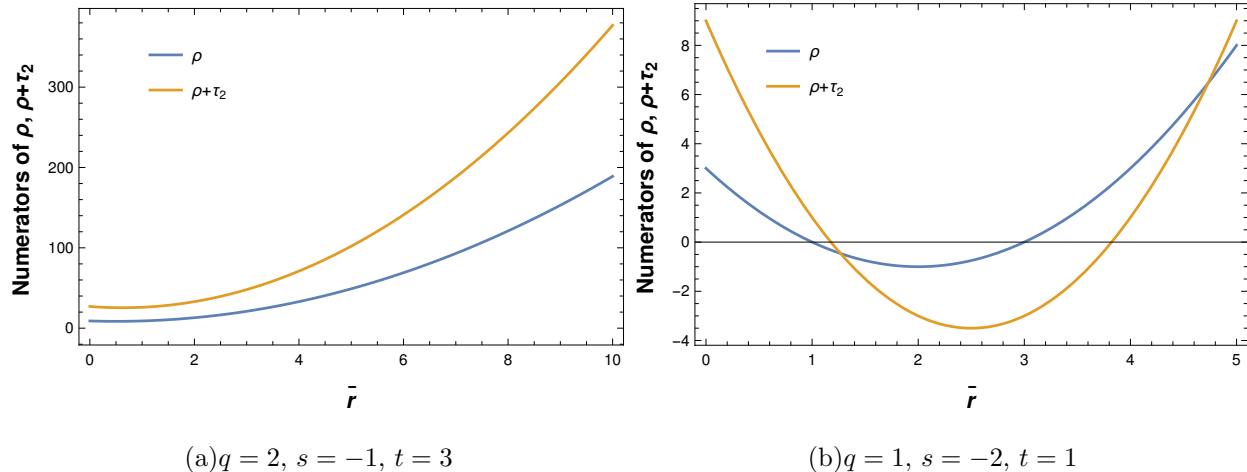


FIG. 2: Numerators of energy condition inequalities: $\rho \geq 0$ inequality (blue), $\rho + \tau_2 \geq 0$ inequality (yellow) are plotted as the function of \bar{r} . Note the violation for values not satisfying $s^2 < \frac{72}{25}qt$ (figure on the right).

IV. ANALYSIS OF CRITICAL NULL GEODESICS AND THE RADIUS OF THE SHADOW

When light from a distant astrophysical object or the accretion disk surrounding the black hole arrives in the vicinity of the event horizon, a part of it gets trapped inside the horizon while another part escapes to infinity [23, 26, 78]. This results in the black hole shadow [12] – the two dimensional closed curve in the observer’s sky separating capture and scattering orbits [24, 25, 79]. However, the shadow may not be a direct consequence of the existence of an event horizon [80, 81]. Rather, it is determined by a set of bound null orbits, exterior to the horizon, dubbed as the ‘photon sphere’ in [16] (light rings in [15], photon ring in [82, 83] and critical curve in [79]).

In this section, we study the null geodesics of photons in a general static, spherically symmetric and asymptotically flat line element and first work out the equation of the photon

sphere. Subsequently, we move on to calculate the radius of the black hole shadow (following Bardeen's formalism) in terms of celestial coordinates [15, 24, 84, 85].

Let us begin with the line element

$$ds^2 = g_{\alpha\beta} dx^\alpha dx^\beta = -\mathcal{A}(r) dt^2 + \mathcal{B}(r) dr^2 + r^2 d\theta^2 + r^2 \sin^2 \theta d\phi^2 \quad (4.1)$$

such that, $\lim_{r \rightarrow \infty} \mathcal{A}(r) = \lim_{r \rightarrow \infty} \mathcal{B}(r) = 1$. The Lagrangian describing the motion of photons in this metric is

$$2 \mathcal{L}(x^\alpha, \dot{x}^\alpha) = g_{\alpha\beta} \dot{x}^\alpha \dot{x}^\beta \quad (4.2)$$

where \dot{x}^α is the tangent vector along a curve $x^\alpha = x^\alpha(\lambda)$, where λ is the affine parameter. The conjugate momentum corresponding to the coordinate x^α is p_α . Since the metric is independent of t and ϕ , the corresponding constants of motion are the energy E and the angular momentum L . By solving these two expressions we can get the geodesic equations corresponding to t and ϕ coordinates. The Hamiltonian for the photons is

$$\mathcal{H} = \frac{1}{2} g^{\alpha\beta} p_\alpha p_\beta = 0 \quad (4.3)$$

The geodesic equations corresponding to r and θ coordinates can be obtained from the Hamilton-Jacobi equation

$$\mathcal{H}(x^\alpha, p_\alpha) + \frac{\partial \mathcal{S}}{\partial \lambda} = 0 \quad (4.4)$$

The Jacobi action \mathcal{S} is integrated with the help of the two known constants of motion and is of the following form

$$\mathcal{S} = -E t + L \phi + \bar{\mathcal{S}}(r, \theta) \quad (4.5)$$

For the given static, spherically symmetric metric, $\bar{\mathcal{S}}(r, \theta)$ happens to be separable in r and θ , i.e., $\bar{\mathcal{S}}(r, \theta) = \mathcal{S}^r(r) + \mathcal{S}^\theta(\theta)$. The 'r' and ' θ ' components of the momentum are, respectively, p_r and p_θ . Inserting p_r and p_θ in the Hamilton-Jacobi equation, and separating out the parts corresponding to r and θ coordinates, we get

$$\left[\frac{1}{\mathcal{B}} \left(\frac{d\mathcal{S}^r}{dr} \right)^2 - \frac{E^2}{\mathcal{A}} \right] r^2 + L^2 = - \left(\frac{d\mathcal{S}^\theta}{d\theta} \right)^2 - L^2 \cot^2 \theta = -K, \quad (4.6)$$

where K is a separation constant, also known as the Carter constant [86], representing the third constant of motion. Thus, geodesic equations corresponding to r and θ coordinates are

$$\mathcal{B}(r) \dot{r} = E \sqrt{\mathcal{B} \left[\frac{1}{\mathcal{A}} - \frac{\ell^2 + \chi}{r^2} \right]} = E \sqrt{-V(r)}, \quad (4.7)$$

$$\dot{\theta} = \frac{E}{r^2} \sqrt{\Theta(\theta)}, \quad (4.8)$$

where $\ell = \frac{L}{E}$, $\chi = \frac{K}{E^2}$ and $\Theta(\theta) = \chi - \ell^2 \cot^2 \theta$, while the effective potential in which the photons move is given as,

$$V(r) = \mathcal{B} \left[\frac{\ell^2 + \chi}{r^2} - \frac{1}{\mathcal{A}} \right]. \quad (4.9)$$

The radii of the photon sphere r_{ph} correspond to the highest maximum of the effective potential $V(r)$ subject to the following conditions

$$V(r_{\text{ph}}) = 0, \quad V'(r_{\text{ph}}) = 0, \quad V''(r_{\text{ph}}) < 0 \quad (4.10)$$

From Eq.(4.10) we get the following conditions

$$\chi + \ell^2 = \frac{r_{\text{ph}}^2}{\mathcal{A}(r_{\text{ph}})} \quad \text{and} \quad \chi + \ell^2 = \frac{1}{2} \frac{\mathcal{A}'(r_{\text{ph}})}{\mathcal{A}^2(r_{\text{ph}})} r_{\text{ph}}^3 \quad (4.11)$$

where a prime denotes derivative w.r.t. the radial coordinate r . We determine the photon sphere radius taking the maximum positive root of the following photon sphere equation.

$$\frac{\mathcal{A}'(r_{\text{ph}})}{\mathcal{A}(r_{\text{ph}})} r_{\text{ph}} = 2 \quad (4.12)$$

In order to derive the contour of the black hole shadow in the observer's sky, one considers the projection of the photon sphere in the image plane. The locus of the shadow boundary is expressed in terms of two celestial coordinates. In terms of the tangent to a photon geodesic at the observer's position located at a distance r_0 from the center of the black hole, the celestial coordinates are [15, 24, 84, 85]

$$\alpha = -\frac{\ell}{\sin \theta_0}, \quad \beta = \pm \sqrt{\Theta(\theta_0)}, \quad (4.13)$$

where θ_0 is the inclination angle of the observer with respect to Z -axis of the black hole. The contour of the shadow describes a circle $\alpha^2 + \beta^2 = \chi + \ell^2$. Note that the circular shape of the shadow boundary is true as long as the spacetime is spherically symmetric and static with any functional form of the metric functions $\mathcal{A}(r)$ and $\mathcal{B}(r)$, provided photon spheres and shadows do exist for such metric functions. The actual observational appearance of the shadow on observer's sky may differ from circularity due to the rotation of the black holes and the effect of the presence of the surrounding accretion disk. In [87], the authors analysed the appearance of the shadows of M87* as elliptical, based on the rotation of the black holes and the data sets produced from GRMHD simulations. However, we restrict our discussion here to non-rotating black holes only, for simplicity and also as the observed

shadows do not seem to show a large deviation from circularity. Therefore, the radius of the shadow is given by

$$r_{\text{sh}} = \left(\frac{1}{2} \frac{\mathcal{A}'(r_{\text{ph}})}{\mathcal{A}^2(r_{\text{ph}})} r_{\text{ph}}^3 \right)^{\frac{1}{2}} = \frac{r_{\text{ph}}}{\sqrt{\mathcal{A}(r_{\text{ph}})}} \quad (4.14)$$

The equation of photon sphere is

$$2r_{\text{ph}}^4 + 3\mathcal{P}r_{\text{ph}}^3 + 4\mathcal{Q}r_{\text{ph}}^2 + 5\mathcal{S}r_{\text{ph}} + 6\mathcal{T} = 0 \quad (4.15)$$

The condition for the existence of a horizon is given from the requirement $g_{tt} = 0$ which leads to:

$$r_{\text{hr}}^4 + \mathcal{P}r_{\text{hr}}^3 + \mathcal{Q}r_{\text{hr}}^2 + \mathcal{S}r_{\text{hr}} + \mathcal{T} = 0 \quad (4.16)$$

We will now rewrite the photon sphere equation and the horizon condition using dimensionless quantities mentioned before, i.e.

$$\mathcal{P} = -2M \quad ; \quad \mathcal{Q} = qM^2 \quad ; \quad \mathcal{S} = sM^3 \quad ; \quad \mathcal{T} = tM^4 \quad (4.17)$$

We further define

$$x = \frac{r_{\text{hr}}}{M} \quad ; \quad y = \frac{r_{\text{ph}}}{M} \quad (4.18)$$

With these redefinition the equations for x and y become:

$$x^4 - 2x^3 + qx^2 + sx + t = 0, \quad (4.19)$$

and

$$2y^4 - 6y^3 + 4qy^2 + 5sy + 6t = 0. \quad (4.20)$$

Both these equations now involve dimensionless quantities only. From elementary algebra we know that the cubic terms in the quartic equations can be removed by simple transformations. If we write $x = z_1 + \frac{1}{2}$ and $y = z_2 + \frac{3}{4}$, the equations for z_1 and z_2 turn out to be

$$z_1^4 + \left(q - \frac{3}{2} \right) z_1^2 + (q + s - 1) z_1 + \left(\frac{s}{2} + \frac{q}{4} + t - \frac{3}{16} \right) = 0 \quad (4.21)$$

and

$$z_2^4 + \left(2q - \frac{27}{8}\right) z_2^2 + \left(\frac{5s}{2} + 3q - \frac{27}{8}\right) z_2 + \left(\frac{15s}{8} + \frac{9q}{8} + 3t - \frac{243}{256}\right) = 0 \quad (4.22)$$

We will now explore some special case solutions of these equations and obtain the expressions for the photon sphere, the horizon and the shadow radius as functions of one or more of the parameters q , s and t . In general, one may write

$$r_{hr} = U(q, s, t)M \quad ; \quad r_{ph} = V(q, s, t)M \quad ; \quad r_{sh} = W(q, s, t)M \quad (4.23)$$

where $U(0, 0, 0) = 2$, $V(0, 0, 0) = 3$ and $W(0, 0, 0) = 3\sqrt{3}$ and M in dimensionful form is $\frac{GM}{c^2}$. The general form of the three functions $U(q, s, t)$, $V(q, s, t)$ and $W(q, s, t)$ can, in principle, be obtained by solving for the real roots of the quartic equations quoted above. We confine ourselves below to a study of special cases, largely dictated by (a) the requirements of simplicity and (b) obvious mathematical conditions which lead to simpler and tractable scenarios for which we can find some viable answers.

Case 1: This is the simplest case where we consider the coefficients of z_1 and z_2 as zero. This results in algebraic equations for q and s which have solutions

$$q = \frac{7}{4} \quad ; \quad s = -\frac{3}{4} \quad (4.24)$$

We have seen that the energy conditions will hold provided $S^2 < \frac{72}{25}Q\mathcal{T}$ which, with the q , s , t parametrisation becomes $s^2 < \frac{72}{25}qt$. With $q = \frac{7}{4}$ and $s = -\frac{3}{4}$ this becomes $t > \frac{25}{224}$. With this choice the equations for z_1 , z_2 are reduced to quadratic equations in z_1^2 and z_2^2 . The real solutions of these equations give

$$z_1 = \sqrt{\frac{\sqrt{9 - 64t} - 1}{8}} \quad ; \quad z_2 = \sqrt{\frac{2\sqrt{25 - 192t} - 1}{16}} \quad (4.25)$$

Recalling definitions, we finally obtain

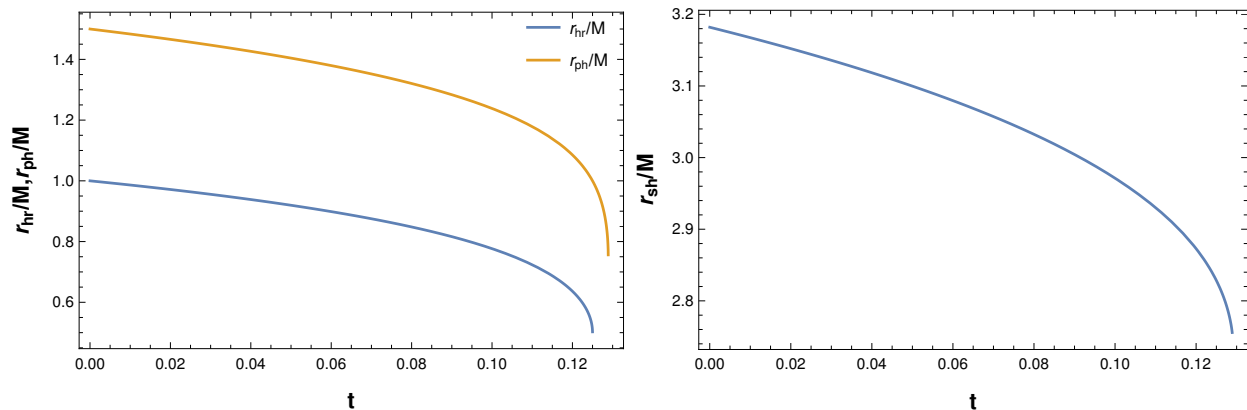
$$r_{hr} = \left(\frac{1}{2} + \sqrt{\frac{\sqrt{9 - 64t} - 1}{8}}\right) M \quad (4.26)$$

$$r_{ph} = \left(\frac{3}{4} + \sqrt{\frac{2\sqrt{25 - 192t} - 1}{16}}\right) M \quad (4.27)$$

Notice that there is a restriction imposed on t in order to have real values for z_1 , z_2 and hence, r_{hr} and r_{ph} . One can verify easily that within this domain $r_{hr} < r_{ph}$ (see Figure 3(a)).

Note that for $t < 0$ energy conditions are satisfied for $r > r_{+,max}$ as we noted earlier (see Table I). One can verify that, for the specific choice of q and s here, the horizon radius r_{hr} is always less than $r_{+,max}$, meaning there is always a violation of energy conditions outside the horizon up to the limit $r_{+,max}$. Further, there is a range of $t > 0$ (i.e. $0.061 < t < 0.1116$) over which one can still satisfy the energy conditions, at least outside the horizon of the spacetime. For $t \geq 25/224$ the energy conditions are satisfied for all r . However, $t > 1/8$ correspond to the naked singularities.

Finally, we need to write down the shadow radius for any t . This is a complicated expression, so we just plot it as a function of t (see Figure 3(b)). Note that photon sphere and the shadow do not exist for the naked singularities for $t > 99/768$.



(a) $\frac{r_{hr}}{M}$ (blue) and $\frac{r_{ph}}{M}$ (yellow) as a function of t (x -axis).

(b) Shadow radius $\frac{r_{sh}}{M}$ as a function of t .

FIG. 3: Horizon radius, photon sphere radius and shadow radius as a function of t for $q = 7/4$, $s = -3/4$. Energy condition satisfying scenario for $t > \frac{25}{224} = 0.111607$. Note that the shadow radius is less than $3\sqrt{3}M$, i.e. lesser than Schwarzschild.

The radius for a fixed M is smaller than that for Schwarzschild, as is evident from the graph. We will need to choose other values of the free parameters in order to make it equal or larger than the Schwarzschild.

Case 2: Another simplifying assumption could be to assume the constant and the coefficients of the linear in the z_1, z_2 terms in the quartic equations to be zero. Since we have three parameters q, s and t one needs three equations. We can either assume both these

coefficients in the z_1 equation to be equal to zero and one of them in the z_2 equation to be zero. The opposite can also be considered. There will be four such choices given as:

(a) $q + s - 1 = 0$, $8s + 4q + 16t = 3$, $20s + 24q - 27 = 0$.

Here $q = \frac{7}{4}$, $s = -\frac{3}{4}$, $t = \frac{1}{8}$. The energy condition requirement $s^2 < \frac{72}{25}qt$ holds. This corresponds to $t = \frac{1}{8}$ in Case 1 given above. Here $z_1 = 0$, hence $r_{\text{hr}} = 0.5M$ and $r_{\text{ph}} = M$. The shadow radius can be read off from the figure.

(b) $q + s - 1 = 0$, $8s + 4q + 16t = 3$, $288q + 480s + 768t - 243 = 0$.

This set does not have a solution for q, s, t .

(c) $q + s - 1 = 0$, $20s + 24q - 27 = 0$, $288q + 480s + 768t - 243 = 0$.

Here $q = \frac{7}{4}$, $s = -\frac{3}{4}$, $t = \frac{33}{256}$. The energy condition requirement holds. The photon sphere here will be at $r_{\text{ph}} = 0.75M$. There is no horizon as the z_1 equation has no real root. Thus, we have a naked singularity. The shadow radius is $r_{\text{sh}} = 2.75568M$.

(d) $8s + 4q + 16t = 3$, $20s + 24q - 27 = 0$, $288q + 480s + 768t - 243 = 0$.

Here $q = \frac{51}{32}$, $s = -\frac{9}{16}$, $t = \frac{9}{128}$. Here also the energy conditions hold good. There are two real roots of the z_1 quartic equation, i.e. $z_1 = 0$ and $z_1 = -0.0104$. Thus this describes a black hole with double horizon, where $z_1 = 0$ for the event horizon and $z_1 = -0.0104$ for the cauchy horizon. Thus, the event horizon is at $r_{\text{hr}} = 0.5M$. The photon sphere equation has the solutions $z_2 = 0$ and $z_2 = \pm\frac{\sqrt{3}}{4}$. One can verify that only $z_2 = \frac{\sqrt{3}}{4}$ corresponds to the unstable photon orbit outside the event horizon. Thus the radius of the photon sphere is $r_{\text{ph}} = \frac{(3+\sqrt{3})M}{4}$ and the shadow radius $r_{\text{sh}} = 3.11386M$.

Case 3 (General): We now go back to the quartic equations for z_1 and z_2 , i.e. (4.21) and (4.22). Is it possible to arrive at some general analytical results on the roots? Following early work by Arnon [88] (see also another recent article [89]) we are able to extract the following information which we state below.

Let us assume the quartic equation in the form

$$u^4 + au^2 + bu + c = 0 \tag{4.28}$$

We further define two quantities

$$\delta(a, b, c) = 256c^3 - 128a^2c^2 + 144ab^2c + 16a^4c - 27b^4 - 4a^3b^2, \tag{4.29}$$

$$L(a, b, c) = 8ac - 9b^2 - 2a^3. \tag{4.30}$$

Real roots of the quartic will exist for specific conditions on δ and L . In fact, the multiplicity of the real root can also be obtained. The list appears in [88] and [89]. We mention the conditions of interest to us:

(a) The condition for no real roots is $(\delta > 0 \text{ and } (L \leq 0 \text{ or } a > 0)) \text{ OR } (\delta = 0 \text{ and } L = 0 \text{ and } a > 0)$.

(b) The condition for two distinct real roots is just $\delta < 0$.

Six other conditions are stated in [88] and [89].

We will use (a) for z_1 to find examples of spacetimes without horizons, i.e. those with a naked singularity. We can use (a) for z_2 to show there are no photon spheres and hence no shadow. With (b) we can find horizons and photon spheres. In particular, if we have one positive and one negative root we can use the obvious fact that $r > 0$ in order to throw away the negative root. That will leave us, from (b), with one horizon and one photon sphere.

In Fig. 4, we show s vs. q region plots for the chosen values of t . Each panel of the figure shows three shaded regions with uniform grey colour density but different boundary colours, i.e. black, blue, and red, signifying three different characteristics as mentioned in the figure. The region with black boundary satisfies the NEC and WEC, whereas the region outside do not satisfy the energy conditions. The shaded region under the blue boundary correspond to the naked singularities and the outside region is for the black holes. For the shaded region under the red boundary, photon spheres as well as the shadows do not exist. Note that the red boundary never crosses the blue boundary, meaning the non-existence of photon spheres only correspond to the naked singularities. However, there are overlaps of the parts of these three shaded regions—in the darker patches the overlap is more. There are the overlapping regions **A** for the black holes and **B** for the naked singularities, where the photon spheres exist and also the energy conditions are satisfied. In **C**, where parts of all the three shaded regions overlap, photon spheres and shadows do not exist although the energy conditions are satisfied. As the t values are increased as shown in the different panels of the figure, the region **A** and **B** become thinner in the direction of q but lengthier along s , i.e. for a given choice of q the allowed range of s increases, but for a given choice of s the allowed range of q decreases. In Table II, we demonstrate these facts with specific choices of q , s , and t . We take all possible combinations of $q = \{\frac{1}{2}, \frac{4}{3}\}$, $s = \{-\frac{1}{3}, -\frac{1}{10}\}$, and $t = \{\frac{1}{100}, \frac{1}{10}\}$ and compute the horizon radius, shadow radius, and check the energy conditions explicitly, thereby verifying their correspondence with the Fig. 4.

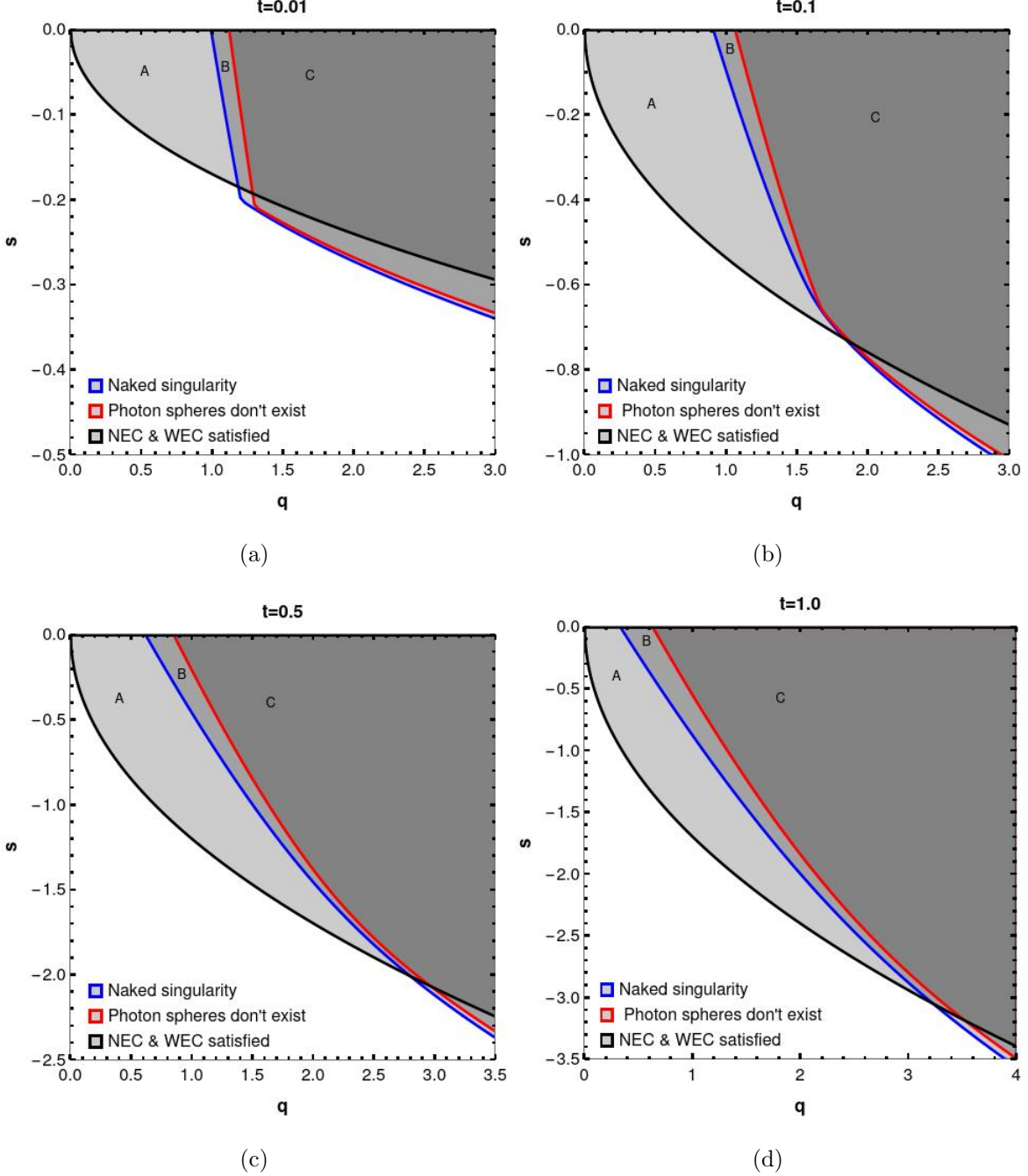


FIG. 4: q vs. s region plot for fixed $t > 0$. Note that we choose the domain $q > 0$ and $s < 0$. The shaded region with blue boundary correspond to naked singularities (the rest is for the black holes), the shaded region under the black boundary satisfies the energy conditions at all r , i.e. $s^2 < \frac{72}{25}qt$, and for the shaded region with red boundary, photon spheres do not exist. The overlapping regions **A** and **B** correspond to allowed black holes and naked singularities respectively for which the energy conditions are satisfied and also the photon spheres exist. In the region **C** the photon spheres do not exist though energy conditions are satisfied.

| (q, s, t) | (δ_1, L_1) | (δ_2, L_2) | (z_1, z_2) | r_H (in M) | r_{ph} (in M) | r_{sh} (in M) | $s^2 < \frac{72}{25}qt?$ |
|---|-------------------|-------------------|---------------------------|--------------|-----------------|-----------------|--------------------------|
| $(\frac{1}{2}, -\frac{1}{10}, \frac{1}{100})$ | $< 0, < 0$ | $< 0, < 0$ | (1.24434, 1.90751) | 1.74434 | 2.65751 | 4.74945 | <i>Yes</i> |
| $(\frac{1}{2}, -\frac{1}{10}, \frac{1}{10})$ | $< 0, < 0$ | $< 0, < 0$ | (1.22413, 1.8909) | 1.72413 | 2.6409 | 4.73556 | <i>Yes</i> |
| $(\frac{1}{2}, -\frac{1}{3}, \frac{1}{100})$ | $< 0, < 0$ | $< 0, < 0$ | (1.32444, 1.99484) | 1.82444 | 2.74484 | 4.83878 | <i>No</i> |
| $(\frac{1}{2}, -\frac{1}{3}, \frac{1}{10})$ | $< 0, < 0$ | $< 0, < 0$ | (1.30854, 1.98082) | 1.80854 | 2.73082 | 4.82672 | <i>Yes</i> |
| $(\frac{4}{3}, -\frac{1}{10}, \frac{1}{100})$ | $> 0, < 0$ | $> 0, < 0$ | (<i>None, None</i>) | <i>None</i> | <i>None</i> | <i>None</i> | <i>Yes</i> |
| $(\frac{4}{3}, -\frac{1}{10}, \frac{1}{10})$ | $> 0, < 0$ | $> 0, < 0$ | (<i>None, None</i>) | <i>None</i> | <i>None</i> | <i>None</i> | <i>Yes</i> |
| $(\frac{4}{3}, -\frac{1}{3}, \frac{1}{100})$ | $< 0, > 0$ | $< 0, > 0$ | (0.465475, 0.982887) | 0.965475 | 1.73289 | 3.63773 | <i>No</i> |
| $(\frac{4}{3}, -\frac{1}{3}, \frac{1}{10})$ | $> 0, < 0$ | $< 0, < 0$ | (<i>None</i> , 0.775662) | <i>None</i> | 1.52566 | 3.53269 | <i>Yes</i> |

TABLE II: Specific illustrative examples of the general case. Each entry can be easily correlated with the Fig. 4(a) and Fig. 4(b) and the conditions on the Eqs. (4.29) and (4.30); (δ_1, L_1) and (δ_2, L_2) correspond to the quartic equations of z_1 and z_2 respectively.

V. LINK WITH OBSERVATIONAL RESULTS FROM M87* AND SGRA*

It is known from the EHT observations that the shadow radius for the supermassive compact object (black hole) in the M87 galaxy [1] and Sgr A* (in the center of our galaxy) [6], correspond to angular diameters $42 \pm 3 \mu\text{as}$ and $48.7 \pm 7 \mu\text{as}$, respectively. Assuming the Schwarzschild black hole model, we can obtain the shadow radius using the formula $r_{sh} = \frac{3\sqrt{3}GM}{c^2}$ for the given masses and distances of these objects. The angular diameter value for the black hole in M87 turns out to be $39.6 \mu\text{as}$ (considering the mass $M = 6.5 \times 10^9 M_\odot$ and the distance $D = 16.8 \text{Mpc}$). For Sgr A*, the Schwarzschild value is around $51.2 \mu\text{as}$ (considering the mass $M = 4 \times 10^6 M_\odot$ and the distance $D = 8 \text{Kpc}$). We will now see if the r_{sh} for the line element proposed here can match the observations within error bars. In other words, we ask– what values of q, s, t can yield a shadow radius close or equal to the value found in observations.

For M87*, the angular diameter can be close to the observed value provided the $3\sqrt{3}$ factor is replaced by numerical values ranging from 4.94 (lower bound 39μ) as to 5.71 (upper bound $45 \mu\text{as}$). In the case of SgrA* the corresponding values are: 4.1 (for $41.7 \mu\text{as}$) and 5.46 (for $55.7 \mu\text{as}$). We show below that there does exist (q, s, t) values for which one can

safely say that observations match with theory.

We first consider the case with s negative and $q = t = -s$. The energy conditions obviously hold good without any further restrictions. The roots z_1, z_2 are found as functions of q and thereafter r_{hr}, r_{ph} and r_{sh} are also obtained as functions of q . The expressions are long and complicated and are therefore not quoted here. However, one can check that $q \leq 1.1169$ for black holes, otherwise they are naked singularities.

The figures below (Fig. 5 and Fig. 6) show the possibilities and the q values for which a match with M87* and SgrA* observations is feasible. We note, that the horizon radius is always smaller than the photon sphere radius. The metrics in general are:

$$g^{rr} = -g_{tt} = \left(1 - \frac{2M}{r} + \frac{qM^2}{r^2} - \frac{qM^3}{r^3} + \frac{qM^4}{r^4}\right) \quad (5.1)$$

One can identify the above line element with a Kiselev black hole with appropriately chosen K_i . The range of q in the graphs is chosen to avoid any jumps in the curves which may occur due to pathologies in the roots for certain q values. The allowed q values are the ones for which the shadow radius lies in the observational green band in the figures.

For the black hole M87*, observational limit is $q \leq 0.35$ (see Fig. 5(a)) obtained from the earlier version of the observational range of the angular shadow diameter. However, the new improved (PRIMO) version [90] of the range of angular diameter puts a more stringent limit $q \leq 0.0145$.

For the black hole SgrA*, the EHT papers [6, 11] provide two observational data for the angular diameter. One is mentioned as emission ring diameter $51.8 \pm 2.3 \mu\text{as}$ and the other one is mentioned as the shadow diameter $48.7 \pm 7 \mu\text{as}$. We consider both as the observed shadow diameter and obtain the constraints on the q parameter. From Fig. 6.(a) we find that $q \leq 0.472$ whereas $q \leq 1.268$ from Fig. 6.(b). The latter bound on q implies the possibility of SgrA* being a naked singularity as well. We scrutinize this possibility further using the constraint on fractional deviation parameter (δ) which signals a deviation from the Schwarzschild black hole.

The recent EHT papers on SgrA* observations have used the fractional deviation parameter δ to constrain the spacetime geometries different from the Schwarzschild or Kerr black holes. The definition of δ is as follows,

$$\delta = \frac{d_{sh}}{d_{sh,Sch}} - 1 = \frac{R_{avg}}{3\sqrt{3}M} - 1, \quad (5.2)$$

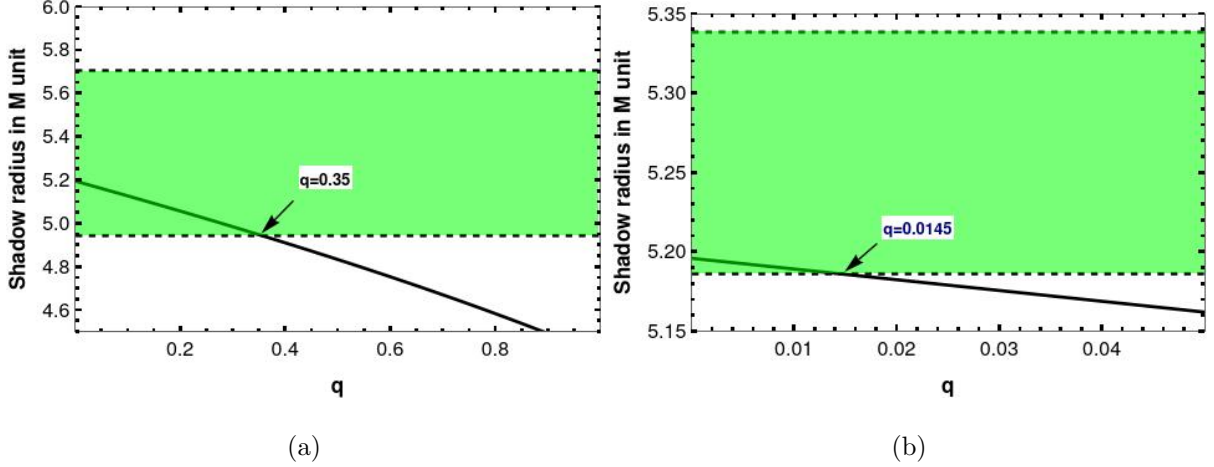


FIG. 5: Shadow radius (r_{sh}) in M units vs. q plot (black solid curve) for the case $q = -s = t$. The green band is the observational range for the black hole M87*. In the plot (a), we take earlier version of the angular shadow diameter range $42 \pm 3 \mu\text{as}$. In the plot (b), we take the new updated (PRIMO) version of the range $41.5 \pm 0.6 \mu\text{as}$. The dashed lines are the upper and lower limits of the observational range.

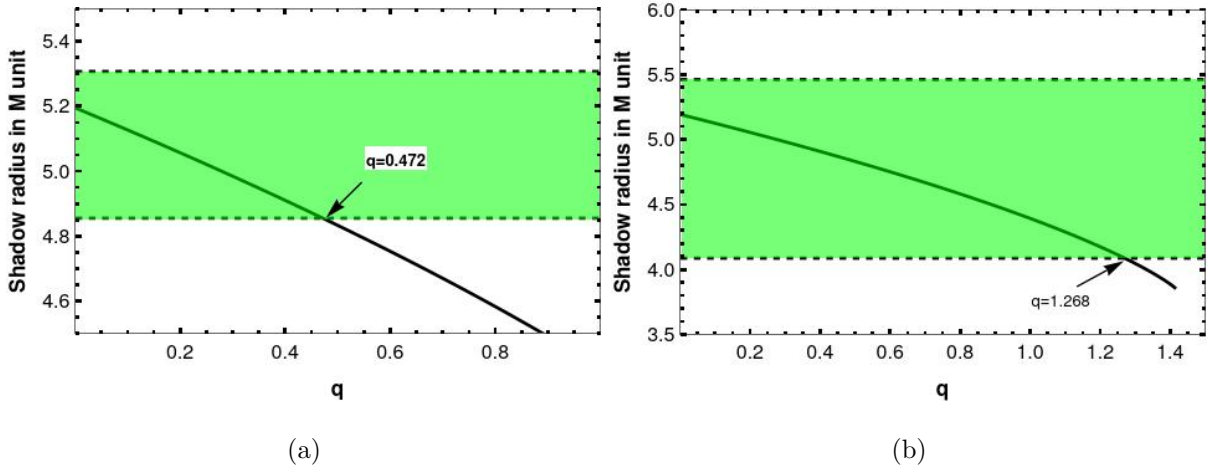


FIG. 6: Shadow radius (r_{sh}) in M units vs. q plot (black solid curve) for the case $q = -s = t$. The green band is the observational range for the black hole SgrA*. In the plot (a), we take the angular (emission) ring diameter range $51.8 \pm 2.3 \mu\text{as}$. In the plot (b), we take the angular shadow diameter range $48.7 \pm 7 \mu\text{as}$. The dashed lines are the upper and lower limits of the observational range.

where the average diameter of the shadow, $d_{sh} = 2R_{avg}$. Using the observations of the shadow of SgrA* and two separate sets of prior values of mass and distance of SgrA* from the VLTI and Keck observations, the EHT collaboration provided the bound on δ [6, 11] as

$$\delta = \begin{cases} -0.08_{-0.09}^{+0.09} & \text{(VLTI)} \\ -0.04_{-0.10}^{+0.09} & \text{(Keck)} \end{cases} \quad (5.3)$$

Therefore, combining both these bounds, we have $-0.14 < \delta < 0.01$. Using this constraint we obtain observational limit $q \leq 0.93$ (see Fig. 7). Considering all the obtained bounds on q together, we get the best possible one, $q \leq 0.472$, for the black hole SgrA*, with the present accuracy of available data. However, it is expected that improved values will appear when the PRIMO technique is applied to the data for SgrA*.

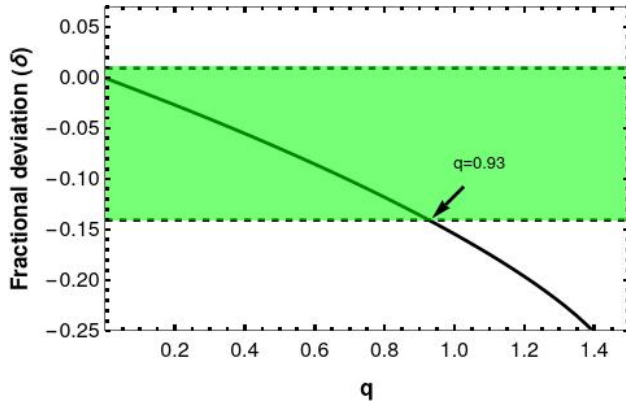


FIG. 7: $q = -s = t$, $q > 0$. q is on the x-axis. The y-axis represents the fractional deviation parameter δ . The black solid line is the theoretical. The green band bounded by lower and upper dashed lines is observational range for the black hole SgrA* from VLTI and Keck bounds.

In order to facilitate a comparison with the metric that arises in Rastall gravity we must try and see what happens if either the term in $\frac{1}{r^3}$ or the term in $\frac{1}{r^4}$ is nonzero. For the term $\frac{1}{r^3}$ we look at the case $t = 0$ but $s \neq 0$, and, for the term $\frac{1}{r^4}$, we look at $s = 0$ but $t \neq 0$. We scan the parameter space q vs s and q vs t respectively for the cases with $\frac{1}{r^3}$ and $\frac{1}{r^4}$. In Figs. 8, 9, 10, 11, we show the contour plots in the parameter space. The allowed regions are specified by the contour lines marked with the observational values. One can see from the metric in Eq. (2.7) that for $\kappa\lambda = \frac{2}{3}$ one retains the term in $\frac{1}{r^3}$ and for $\kappa\lambda = \frac{1}{2}$ one retains the term in $\frac{1}{r^4}$. Thus the shadow corresponding to the metric in Rastall gravity can also be modeled with a suitable choice of parameters in a special case of our general line element.

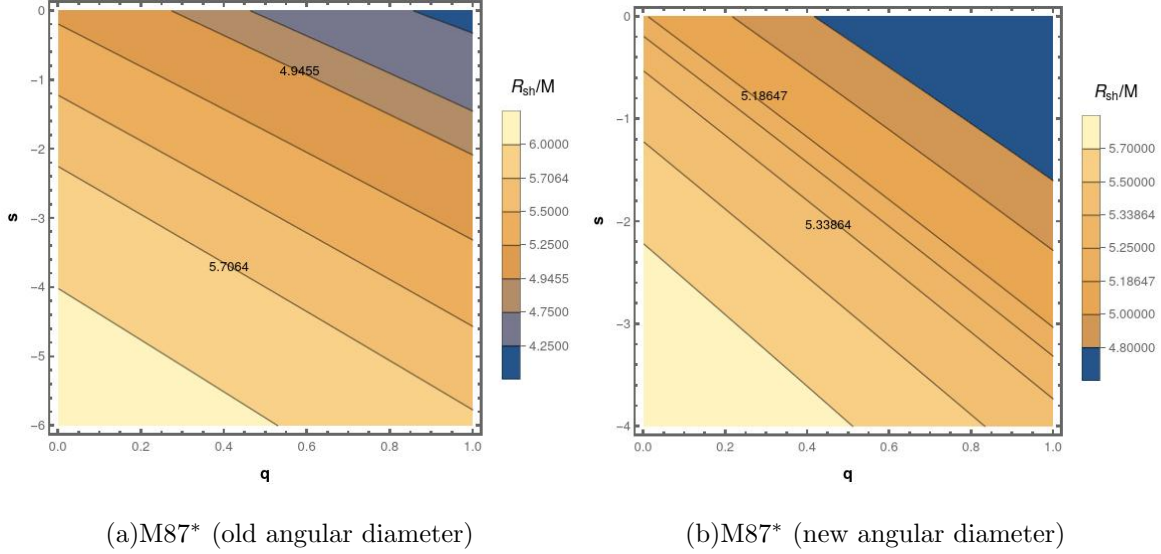


FIG. 8: q vs. s contour plots for the case $t = 0$ (for M87*). The area bounded by the marked contour lines are only allowed in each plot. In the plot (a), we take earlier version of the angular shadow diameter range $42 \pm 3 \mu\text{as}$ for the M87*. Contours represent the fixed values of the shadow radius in the mass unit. The observational limits on the shadow radius are marked on the specific contours in the plot. In the plot (b), we take the new updated (PRIMO) version of the range $41.5 \pm 0.6 \mu\text{as}$ for the M87*.

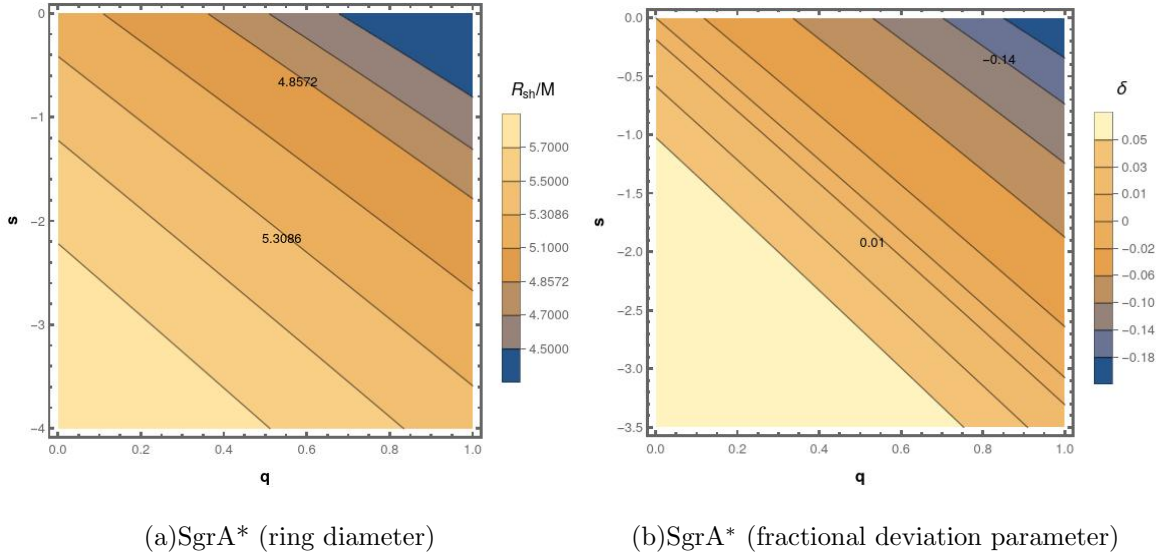
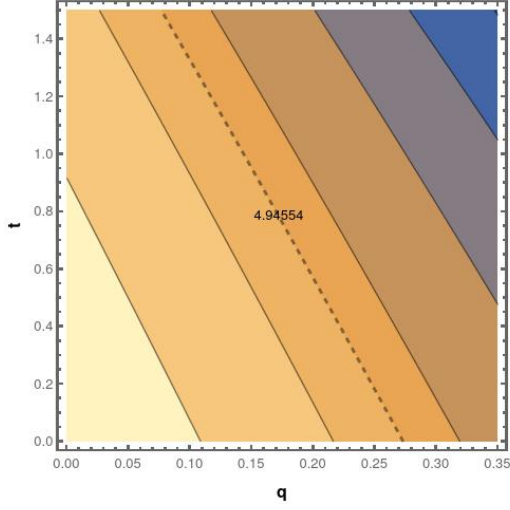
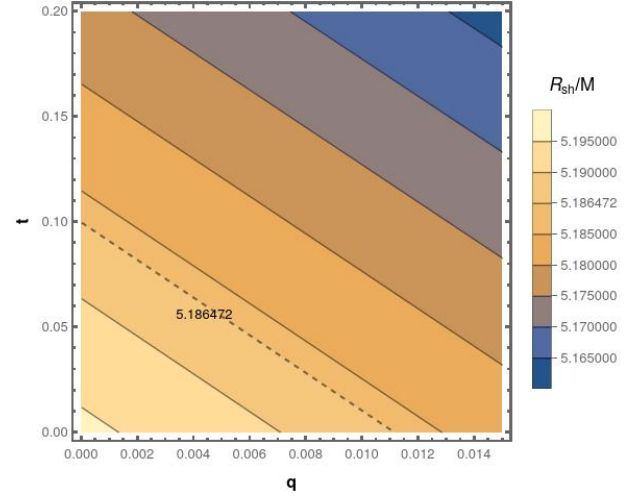


FIG. 9: q vs. s contour plots for the case $t = 0$ (for SgrA*). In the plot (a), the angular (emission) ring diameter range $51.8 \pm 2.3 \mu\text{as}$ is considered for the SgrA*. In the plot (b), we use the observational range for the fractional deviation parameter (δ) for the SgrA*. Here, the contours represent the fixed values of δ with the observational ones are marked on the plot.

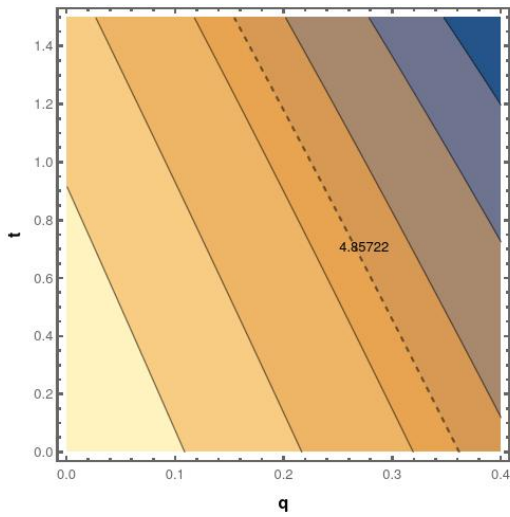


(a)M87* (old angular diameter)

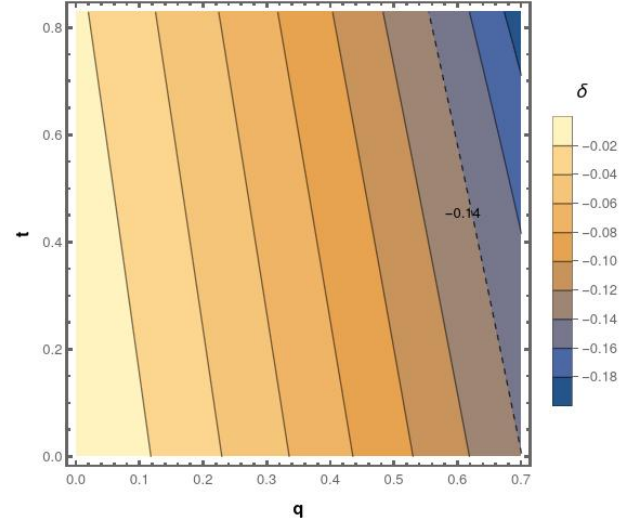


(b)M87* (new angular diameter)

FIG. 10: q vs. t contour plots for the case $s = 0$ (for M87*).



(a)SgrA* (ring diameter)



(b)SgrA* (fractional deviation parameter)

FIG. 11: q vs. t contour plots for the case $s = 0$ (for SgrA*).

It is also possible to consider more general cases where all of q , s , and t take non-zero values. For example, one can choose a specific value of t and then analyze the parameter space q vs. s for the allowed region.

VI. A MORE GENERAL METRIC AND CONSEQUENCES

Let us now consider a more general metric (arbitrary but finite N) for which the g_{tt} and g_{rr} are given as:

$$g_{tt} = - \left(1 + \sum_{n=1}^N \frac{a_n}{r^n} \right) = - \frac{1}{g_{rr}} \quad (6.1)$$

Here a_n are the generalisations of the $\mathcal{P}, \mathcal{Q}, \mathcal{R}, \mathcal{T}$ discussed just above.

We begin with the photon sphere equation in this metric which turns out to be

$$2 r_{\mathbf{ph}}^N + \sum_{n=1}^N a_n (n+2) r_{\mathbf{ph}}^{N-n} = 0 \quad (6.2)$$

On the other hand the horizon equation for the general case is

$$r_{\mathbf{hz}}^N + \sum_{n=1}^N a_n r_{\mathbf{hz}}^{N-n} = 0 \quad (6.3)$$

Below we discuss two special solutions of the general case.

(a) First we assume a special choice wherein the general photon sphere equation (6.2) reduces to the form

$$(r_{\mathbf{ph}} - p)^N = r_{\mathbf{ph}}^N - N r_{\mathbf{ph}}^{N-1} p + \dots + (-1)^N p^N = 0. \quad (6.4)$$

This means that the photon sphere is located at $r_{\mathbf{ph}} = p$. Of course this will happen only for a specific set of a_n in the original metric. Comparing the two photon sphere equations (i.e. 6.2 and 6.4) one finds that

$$a_n = (-1)^n \frac{2N!}{n! (N-n)! (n+2)} p^n \quad (6.5)$$

The general metric now takes on a special form with

$$g_{tt} = - \left(1 + \sum_{n=1}^N \frac{2(-1)^n N!}{n! (N-n)! (n+2)} \left(\frac{p}{r} \right)^n \right) = - \frac{1}{g_{rr}} \quad (6.6)$$

It is now easy to write down the shadow radius $r_{\mathbf{sh}}$, which, after some straightforward algebra becomes

$$r_{\mathbf{sh}} = \sqrt{\frac{(N+1)(N+2)}{2}} p \quad (6.7)$$

One can check that the two inequalities $\rho \geq 0$ and $\rho + \tau_i \geq 0$ for satisfying the WEC and NEC, reduce to the following:

$$\sum_{n=1}^N \frac{2(-1)^{n+1}(1-n)N!}{n!(N-n)!(n+2)} \frac{p^n}{r^{n+2}} \geq 0 \quad (6.8)$$

$$\sum_{n=1}^N \frac{(-1)^{n+2}(n-1)N!}{n!(N-n)!} \frac{p^n}{r^{n+2}} \geq 0 \quad (6.9)$$

Thus, one will need to check the energy conditions for different N (or, if possible for a general N directly) and also find out if the spacetime has horizons and where the horizon is located. Let us quickly check what happens for $N = 4$. For this case, we find

$$g_{tt} = - \left(1 - \frac{8p}{3r} + \frac{3p^2}{r^2} - \frac{8p^3}{5r^3} + \frac{p^4}{3r^4} \right) \quad (6.10)$$

A straightforward calculations shows that there are no horizons and the geometry represents a naked singularity. The shadow radius is given as:

$$r_{\text{sh}} = \sqrt{15} p \quad (6.11)$$

The energy condition inequalities lead to the relations

$$\frac{15r^2p^2 - 16p^3r + 5p^4}{r^6} \geq 0 \quad (6.12)$$

$$\frac{6p^2r^2 - 8p^3r + 3p^4}{r^6} \geq 0 \quad (6.13)$$

One may verify (use $\frac{r}{p}$ as a variable) that both these inequalities hold good and the energy conditions are satisfied for all r .

One can define $p = \nu \frac{GM}{c^2}$ in order to bring in the right dimensions and the mass dependence. It is also instructive to look at what happens for $N = 1$ —this is the simple case of the vacuum Schwarzschild spacetime for which

$$g_{tt} = - \left(1 - \frac{2p}{3r} \right) = - \frac{1}{g_{rr}} \quad (6.14)$$

Choosing $p = \frac{3GM}{c^2}$ one ends up with the standard form of the metric and the shadow radius also reduces to the well-known $3\sqrt{3}\frac{GM}{c^2}$.

(b) We obtain another special solution by making a choice for the form of the general horizon equation (6.3)

$$(r_{\text{hz}} - e)^N = 0, \quad (6.15)$$

where the horizon equation has the only root ‘e’ (here e is not the Euler number, but any arbitrary positive quantity) with multiplicity N. Then the coefficients of the general metric take the form

$$a_n = (-1)^n \frac{N!}{n!(N-n)!} e^n, \quad (6.16)$$

and the resulting metric components are

$$g_{tt} = - \left(1 - \frac{e}{r}\right)^N = -g_{rr}^{-1}. \quad (6.17)$$

The spacetime represents a generic version of the extremal Reissner-Nordström (RN) black holes. For $N = 2$ we recover a RN black hole with mass $M = e$ and the charge $Q = \pm e$ (note that e must be positive for a black hole). For $N = 4$, the metric component takes the form

$$g_{tt} = - \left(1 - \frac{4e}{r} + \frac{6e^2}{r^2} - \frac{4e^3}{r^3} + \frac{e^4}{r^4}\right), \quad (6.18)$$

where the mass of the black hole is then $M = 2e$ and the effective charge $Q = \pm\sqrt{6}e$. The shadow radius for such a class of extremal black holes is given by

$$r_{\text{sh}} = e \left(1 + \frac{N}{2}\right) \left(1 + \frac{2}{N}\right)^{\frac{N}{2}}. \quad (6.19)$$

The validity of NEC and WEC leads to the inequality

$$\left[1 + \frac{e}{r - e}\right]^N - \left[1 + \frac{eN}{r - e}\right] \geq 0, \quad (6.20)$$

which is satisfied for all $r \geq e$, i.e. outside the horizon.

VII. CONCLUSIONS

Schwarzschild and Reissner-Nordström spacetimes are the simplest and most widely used representatives of spherically symmetric, static black holes. In this paper, we have considered a more general static, spherisymmetric spacetime in the Schwarzschild gauge, by considering a general series involving $\frac{1}{r^k}$ ($k \geq 0$) terms, with arbitrary constant coefficients, in the metric functions. Such a metric may be a solution in GR coupled with matter fields or may be a solution in a modified/ alternative theory of gravity. It could also represent black holes or other real or hypothetical objects in astrophysics. We have first analyzed the energy conditions (NEC and WEC) for the matter required (assuming the Einstein field equations

of GR), if such a general spacetime has to exist. Thereafter, we restrict the parameter space of our line element by comparing the size of the circular shadow profile with observational data for M87* and SgrA*.

Our generic metric (2.1) is parametrized by four (assuming terms upto $\frac{1}{r^4}$) constants \mathcal{P} , \mathcal{Q} , \mathcal{S} , \mathcal{T} , where the effective mass and charge of the black hole/ naked singularity are related as $\mathcal{P} = 2M_{\text{eff}}$ and $Q_{\text{eff}} = \pm\sqrt{\mathcal{Q}}$. Analysis of the energy conditions reveal that NEC and WEC are satisfied for all r for any of the following two conditions only: (i) $\mathcal{Q}, \mathcal{S}, \mathcal{T} > 0$, and (ii) $\mathcal{Q} > 0, \mathcal{S} < 0, \mathcal{T} > 0$, and $\mathcal{S}^2 \leq \frac{72}{25}\mathcal{Q}\mathcal{T}$. The first condition implies a naked singularity only and, for the second condition, the spacetime may be a black hole or a naked singularity. For any other choice of the parameters the energy conditions are partially or completely violated. The details are provided in Table I and Fig. 1.

Next we study the critical null geodesic (i.e. photon sphere) and the shadow. We obtain a quartic horizon equation (4.21) and a quartic photon sphere equation (4.22) for the general case. By a root analysis, we scan the parameter space to identify viable regions for black holes/naked singularities and the existence of photon spheres, along with the energy conditions (see Fig. 4 and the Table II for illustration). We also demonstrate some special solutions of the horizon and photon sphere equations.

Thereafter, we compare the observed angular diameters of the M87* and SgrA* with the theoretical prediction for different parameter values satisfying the energy conditions. In particular, we choose $q = -s = t$ (for which the metric takes the form (5.1)). For this metric, comparing with all observations, we get a bound on $q \leq 0.0145$ for M87* (with updated PRIMO data) and $q \leq 0.472$ for SgrA*. We also scan q vs. s parameter space ($t = 0$ for $1/r^3$ term) in Figs. 8, 9 and q vs. t parameter space ($s = 0$ for $1/r^4$ term) in Figs. 10, 11 for observationally allowed regions. Similar plots may also be obtained for more general cases where $q, s, t \neq 0$.

Finally, we try to further generalize the metric functions by including higher order terms $\frac{1}{r^N}$ where N is arbitrary but integral, positive, and finite. However, for arbitrary N and the corresponding constant coefficients, any known simple solution with viable matter fields is not really known. We obtain two special solutions for which either the photon sphere equation or the horizon equation has a single root with multiplicity N . In the first case, for $N = 4$, the solution turns out to be naked singularity whereas in the second case, the solution (for $N = 4$) seems to bear a resemblance (via $M = 2e$) to an extremal Reissner-Nordström

black hole but with higher powers of $\frac{1}{r}$ included.

In the section II, we provided some specific examples which are indeed special cases of the general metric quoted in Eqn. (2.1). In particular, we noted how such special cases of the general metric may represent black holes or naked singularities surrounded by some fluids, namely the Kiselev type solutions both in GR and modified gravity or other solutions as known in diverse contexts. As mentioned before, there do exist many more line elements which fall within the broad class assumed in Eqn. (2.1). Thus, our generic results on energy conditions and shadows may help in understanding features associated with specific line elements which have arisen in different theories of gravity, over the years. It may however be necessary to extend our analysis here, if further higher order terms in $\frac{1}{r}$ have to be considered in the metric functions. Inclusion of such terms will not change the circular shape of the shadow – it will only make the equations more complicated (higher degree polynomials).

Finally, one possible and natural extension of our work is to include rotation, i.e. construct a line element with rotation. One way to do this is to employ the Newman-Janis method [91, 92] of generating rotating spacetimes from static ones. Once we have the rotating spacetimes we can proceed in the same way, as done in this article and construct the shadow profiles. In such a scenario though, the shadow profiles will be much more complicated (no longer simple circles) and it is likely that one will have to use numerical methods to arrive at any meaningful conclusions. We hope to return to this aspect as well as other, similar questions in our future endeavours.

ACKNOWLEDGEMENTS

Research of SJ is partially supported by the SERB, DST, Govt. of India, through a TARE fellowship grant no. TAR/2021/000354, hosted by the Department of Physics, Indian Institute of Technology Kharagpur.

DATA AVAILABILITY STATEMENT

The manuscript has no data associated with it.

- [1] E. H. T. Collaboration et al., arXiv preprint arXiv:1906.11238 (2019).
- [2] K. Akiyama, A. Alberdi, W. Alef, K. Asada, R. Azulay, A.-K. Baczko, D. Ball, M. Baloković, J. Barrett, D. Bintley, et al., The Astrophysical Journal Letters **875**, L2 (2019).
- [3] K. Akiyama, A. Alberdi, W. Alef, K. Asada, R. Azulay, A.-K. Baczko, D. Ball, M. Baloković, J. Barrett, D. Bintley, et al., The Astrophysical Journal Letters **875**, L3 (2019).
- [4] K. Akiyama, A. Alberdi, W. Alef, K. Asada, R. Azulay, A.-K. Baczko, D. Ball, M. Baloković, J. Barrett, D. Bintley, et al., The Astrophysical Journal Letters **875**, L5 (2019).
- [5] E. H. T. Collaboration et al., arXiv preprint arXiv:1906.11243 (2019).
- [6] E. H. T. Collaboration, The Astrophysical Journal Letters **930**, L12 (2022).
- [7] E. H. T. Collaboration, The Astrophysical Journal Letters **930**, L13 (2022).
- [8] E. H. T. Collaboration, The Astrophysical Journal Letters **930**, L14 (2022).
- [9] E. H. T. Collaboration, The Astrophysical Journal Letters **930**, L15 (2022).
- [10] E. H. T. Collaboration, The Astrophysical Journal Letters **930**, L16 (2022).
- [11] E. H. T. Collaboration, The Astrophysical Journal Letters **930**, L17 (2022).
- [12] H. Falcke, F. Melia, and E. Agol, ApJ Letters **528**, L13 (2000), arXiv:astro-ph/9912263 [astro-ph].
- [13] A. E. Broderick and A. Loeb, The Astrophysical Journal **697**, 1164 (2009).
- [14] V. I. Dokuchaev and N. O. Nazarova, Physics-Uspekhi **63**, 583 (2020).
- [15] P. V. Cunha and C. A. Herdeiro, General Relativity and Gravitation **50**, 1 (2018).
- [16] V. Perlick and O. Y. Tsupko, Phys. Rept. **947**, 1 (2022), arXiv:2105.07101 [gr-qc].
- [17] K. S. Virbhadra and G. F. R. Ellis, Phys. Rev. D **62**, 084003 (2000).
- [18] K. S. Virbhadra and G. F. R. Ellis, Phys. Rev. D **65**, 103004 (2002).
- [19] V. Bozza, Phys. Rev. D **66**, 103001 (2002).
- [20] N. Tsukamoto, Phys. Rev. D **95**, 064035 (2017).
- [21] N. Tsukamoto, Eur. Phys. J. C **83**, 284 (2023), arXiv:2211.04239 [gr-qc].
- [22] R. Shaikh, P. Banerjee, S. Paul, and T. Sarkar, Phys. Rev. D **99**, 104040 (2019).

- [23] J. L. Synge, MNRAS **131**, 463 (1966).
- [24] J. M. Bardeen, in Black Holes (Les Astres Occlus) (1973) pp. 215–239.
- [25] J. P. Luminet, Astron. Astrophys. **75**, 228 (1979).
- [26] P. J. Young, Phys. Rev. D **14**, 3281 (1976).
- [27] V. Perlick, Phys. Rev. D **69**, 064017 (2004).
- [28] A. Abdujabbarov, F. Atamurotov, Y. Kucukakca, B. Ahmedov, and U. Camci, Astrophysics and Space Science **344**, 429 (2013).
- [29] R. Takahashi, The Astrophysical Journal **611**, 996 (2004).
- [30] K. Hioki and K.-i. Maeda, Phys. Rev. D **80**, 024042 (2009).
- [31] J. O. Shipley and S. R. Dolan, Classical and Quantum Gravity **33**, 175001 (2016).
- [32] A. Yumoto, D. Nitta, T. Chiba, and N. Sugiyama, Phys. Rev. D **86**, 103001 (2012).
- [33] F. Atamurotov, B. Ahmedov, and A. Abdujabbarov, Phys. Rev. D **92**, 084005 (2015).
- [34] S. Vagnozzi et al., Class. Quant. Grav. **40**, 165007 (2023), arXiv:2205.07787 [gr-qc].
- [35] L. Amarilla, E. F. Eiroa, and G. Giribet, Phys. Rev. D **81**, 124045 (2010).
- [36] L. Amarilla and E. F. Eiroa, Physical Review D **87**, 044057 (2013).
- [37] F. Atamurotov, A. Abdujabbarov, and B. Ahmedov, Astrophys. Space Sci. **348**, 179 (2013).
- [38] S. Vagnozzi and L. Visinelli, Phys. Rev. D **100**, 024020 (2019).
- [39] P. V. Cunha, C. A. Herdeiro, B. Kleihaus, J. Kunz, and E. Radu, Physics Letters B **768**, 373 (2017).
- [40] G. J. Olmo, J. L. Rosa, D. Rubiera-Garcia, and D. Saez-Chillon Gomez, Class. Quant. Grav. **40**, 174002 (2023), arXiv:2302.12064 [gr-qc].
- [41] J. L. Rosa and D. Rubiera-Garcia, Phys. Rev. D **106**, 084004 (2022), arXiv:2204.12949 [gr-qc].
- [42] J. L. Rosa, P. Garcia, F. H. Vincent, and V. Cardoso, Phys. Rev. D **106**, 044031 (2022).
- [43] J. L. Rosa, C. F. B. Macedo, and D. Rubiera-Garcia, Phys. Rev. D **108**, 044021 (2023).
- [44] R. A. Konoplya, Phys. Lett. B **795**, 1 (2019), arXiv:1905.00064 [gr-qc].
- [45] T. Johannsen and D. Psaltis, The Astrophysical Journal **718**, 446 (2010).
- [46] D. Psaltis, F. Özel, C.-K. Chan, and D. P. Marrone, The Astrophysical Journal **814**, 115 (2015).
- [47] A. E. Broderick, T. Johannsen, A. Loeb, and D. Psaltis, The Astrophysical Journal **784**, 7 (2014).

- [48] Y. Mizuno, Z. Younsi, C. M. Fromm, O. Porth, M. De Laurentis, H. Olivares, H. Falcke, M. Kramer, and L. Rezzolla, *Nature Astronomy* **2**, 585 (2018).
- [49] A. F. Zakharov, *Phys. Rev. D* **90**, 062007 (2014), arXiv:1407.7457 [gr-qc].
- [50] H. Falcke and S. B. Markoff, *Classical and Quantum Gravity* **30**, 244003 (2013), arXiv:1311.1841 [astro-ph.HE].
- [51] E. F. Eiroa and C. M. Sendra, *Eur. Phys. J. C* **74**, 3171 (2014), arXiv:1408.3390 [gr-qc].
- [52] H. Reissner, *Annalen der Physik* **355**, 106 (1916).
- [53] G. Nordström, *Koninklijke Nederlandse Akademie van Wetenschappen Proceedings Series B Physical Sciences* **20**, 1238 (1918).
- [54] S. Alexeyev, B. Latosh, V. Prokopov, and E. Emtsova, *Journal of Experimental and Theoretical Physics* **128**, 720 (2019).
- [55] S. Alexeyev and V. Prokopov, *Journal of Experimental and Theoretical Physics* **130**, 666 (2020).
- [56] G. W. Horndeski, *International Journal of Theoretical Physics* **10**, 363 (1974).
- [57] E. Babichev, C. Charmousis, and A. Lehébel, *Journal of Cosmology and Astroparticle Physics* **2017**, 027 (2017).
- [58] T. Kobayashi, *Reports on Progress in Physics* **82**, 086901 (2019).
- [59] Y. S. Myung and D.-C. Zou, *Physical Review D* **100**, 064057 (2019).
- [60] P. D. Mannheim, *Foundations of Physics* **42**, 388 (2012).
- [61] M. Kalb and P. Ramond, *Phys. Rev. D* **9**, 2273 (1974).
- [62] I. Banerjee, S. Sau, and S. SenGupta, *Physical Review D* **101**, 104057 (2020).
- [63] S. Kar, S. SenGupta, and S. Sur, *Physical Review D* **67**, 044005 (2003).
- [64] V. Kiselev, *Classical and Quantum Gravity* **20**, 1187 (2003).
- [65] M. Visser, *Classical and Quantum Gravity* **37**, 045001 (2020).
- [66] L. Randall and R. Sundrum, *Physical review letters* **83**, 3370 (1999).
- [67] N. Dadhich, R. Maartens, P. Papadopoulos, and V. Rezanian, *Physics Letters B* **487**, 1 (2000).
- [68] T. Jacobson, *Classical and Quantum Gravity* **24**, 5717 (2007).
- [69] M.-A. Dariescu, C. Dariescu, V. Lungu, and C. Stelea, *Phys. Rev. D* **106**, 064017 (2022).
- [70] L. C. N. Santos, F. M. da Silva, C. E. Mota, I. P. Lobo, and V. B. Bezerra, (2023), arXiv:2301.02534 [gr-qc].
- [71] R. Whisker, arXiv preprint arXiv:0810.1534 (2008).

- [72] P. Cañate and S. E. P. Bergliaffa, *Phys. Rev. D* **102**, 104038 (2020).
- [73] Y. Heydarzade and F. Darabi, *Physics Letters B* **771**, 365 (2017).
- [74] R. M. Wald, General relativity (Chicago Univ. Press, Chicago, IL, 1984).
- [75] C. W. Misner, K. S. Thorne, and J. A. Wheeler, Gravitation (Princeton University Press, 2017).
- [76] M. S. Morris and K. S. Thorne, *American Journal of Physics* **56**, 395 (1988).
- [77] P. Boonserm, T. Ngampitipan, and M. Visser, *International Journal of Modern Physics D* **25**, 1650019 (2016).
- [78] S. Chandrasekhar, The mathematical theory of black holes (1983).
- [79] S. E. Gralla, D. E. Holz, and R. M. Wald, *Physical Review D* **100**, 024018 (2019).
- [80] P. V. Cunha, C. A. Herdeiro, and M. J. Rodriguez, *Physical Review D* **97**, 084020 (2018).
- [81] A. B. Abdikamalov, A. A. Abdujabbarov, D. Ayzenberg, D. Malafarina, C. Bambi, and B. Ahmedov, *Physical Review D* **100**, 024014 (2019).
- [82] T. Johannsen and D. Psaltis, *Astrophys. J.* **718**, 446 (2010), arXiv:1005.1931 [astro-ph.HE].
- [83] M. D. Johnson, A. Lupasca, A. Strominger, G. N. Wong, S. Hadar, D. Kapec, R. Narayan, A. Chael, C. F. Gammie, P. Galison, et al., *Science advances* **6**, eaaz1310 (2020).
- [84] S. E. Vazquez and E. P. Esteban, arXiv preprint gr-qc/0308023 (2003).
- [85] A. de Vries, *Classical and Quantum Gravity* **17**, 123 (2000).
- [86] B. Carter, *Phys. Rev.* **174**, 1559 (1968).
- [87] P. Tiede, A. E. Broderick, D. C. M. Palumbo, and A. Chael, *Astrophys. J.* **940**, 182 (2022), arXiv:2210.13499 [astro-ph.HE].
- [88] D. S. Arnon, *Artificial Intelligence* **37**, 37 (1988).
- [89] E. M. Prodanov, *International Journal of Applied and Computational Mathematics* **7**, 218 (2021).
- [90] L. Medeiros, D. Psaltis, T. R. Lauer, and F. Özel, *The Astrophysical Journal Letters* **947**, L7 (2023).
- [91] E. T. Newman and A. I. Janis, *J. Math. Phys.* **6**, 915 (1965).
- [92] E. T. Newman, E. Couch, K. Chinnapared, A. Exton, A. Prakash, and R. Torrence, *Journal of Mathematical Physics* **6**, 918 (1965).